Photoelectron Spectroscopy on Thin Films of Extended Zinc Porphyrazines

D. Pop,* B. Winter, W. Freyer, W. Widdra,† and I. V. Hertel‡

Max-Born-Institut für Nichtlineare Optik und Kurzzeitspektroskopie, Max-Born-Strasse 2A, D-12489 Berlin, Germany

Received: July 30, 2004; In Final Form: February 25, 2005

Photoemission measurements were performed on a series of stepwise benzoannelated zinc porphyrazine molecules in thin films. The electronic structure of *tert*-butyl-substituted zinc tetraazaporphyrin, phthalocyanine, and naphthalocyanine is investigated using mainly EUV synchrotron radiation. A detailed analysis of the zinc satellites in the spectra of the valence region is performed in an attempt to infer the effect of ligand size extension on the metal−ligand interactions. No differences in the character of the bond between zinc and ligand were detected as a function of ligand size. The results are compared with those for the respective metal-free and copper-containing molecules.

1. Introduction

Porphyrazine molecules, including tetraazaporphyrins (TAPs), phthalocyanines (Pc's), and naphthalocyanines (Nc's), have long been known as dyes, and more recently they have been investigated for use in gas sensors, computer read/write disks, electrochromic devices, liquid crystals, photovoltaic and solar cells, sensitizers for photodynamic therapy, photocopying applications, nonlinear optics, and molecular electronics.[1−8] These molecules are also attractive due to their similarity to the natural porphyrins. Porphyrazines contain a central C_8N_8 ring surrounded by four pyrrole groups; hence they differ from porphyrins only by the presence of four meso-nitrogen atoms instead of four methine groups in the central ring. The high chemical versatility of the porphyrazine macrocycle allows for tailoring the electronic structure/properties of the molecule through changes of the ligand and/or the central atom(s).

Because these molecules have great potential for industrial applications and in fundamental research, a detailed understanding of their electronic structures and intramolecular charge transfer processes is essential. We have recently used photoelectron spectroscopy to investigate the electronic structures of a series of metal-free[9] and copper[10] porphyrazines with stepwise increased ligand size: *tert*-butyl-substituted tetraazaporphyrin, phthalocyanine, and naphthalocyanine. The system of copper-containing porphyrazines[10] allowed us to also study the interactions between the ligand and a metal with a $3d^9$ configuration in the molecular ground state. Changes in the character of the Cu−ligand bond as a function of the degree of benzoannelation were thus inferred.[10] In the present work we contrast the previous results with data for Zn *tert*-butyl-substituted tetraazaporphyrin, phthalocyanine, and naphthalocyanine in thin films. The Zn atom has a full 3d shell in the ground state of these molecules. Therefore, the absorption spectra of zinc porphyrazines show no ligand-to-metal and metal-to-ligand charge transfer bands, and these compounds are ideal for studying the electronic states of the reduced symmetry (D_{4h}) ring.[11,12] Even though a large amount of experimental[11,13−20] and theoretical studies[11,12,18,21−29] were carried out for clarifying the electronic structure of zinc porphyrazines, photoemission investigations on these compounds are scarce. Moreover, to the best of our knowledge, no photoemission spectra of the valence region have been previously reported for zinc tetraazaporphyrin or for the respective *tert*-butyl-substituted compound.

Due to the completely filled Zn 3d orbitals, the photoemission spectra of zinc porphyrazines exhibit satellite features that are of different nature (shakeup) as compared to those of similar copper complexes (charge transfer). In addition to changes in the electronic structure, in this paper we study the intensity of the zinc shakeup satellites as a function of ligand size, in an attempt to infer the effect of benzoannelation on the Zn−ligand interactions.

2. Experimental Section

2.1. Materials. The zinc porphyrazine molecules studied in this work are sketched in Figure 1. The chemical names of the molecules, from left to right in the figure, are zinc tetra(*tert*-butyl)porphyrazine (or zinc tetra(*tert*-butyl)tetraazaporphyrin), zinc tetra(*tert*-butylbenzo)porphyrazine (or zinc tetra(*tert*-butyl)-phthalocyanine), and zinc tetra(*tert*-butylnaphtho)porphyrazine (or zinc tetra(*tert*-butyl)naphthalocyanine), respectively. For convenience, we denote these molecules as ZnP0, ZnP1, and ZnP2. "P" symbolizes the porphyrazine unit, and the numbers "0", "1", and "2" represent the number of benzo units fused to each pyrrole group. Accordingly, the metal-free compounds are denoted H_2P0, H_2P1, and H_2P2, respectively. Notice that for no substituent (symbolized by R), the molecules in Figure 1 correspond to zinc tetraazaporphyrin (or porphyrazine) (ZnTAP), zinc phthalocyanine (ZnPc), and zinc naphthalocyanine (ZnNc).

ZnP0, ZnP1, and ZnP2 were synthesized from their corresponding metal-free compounds,[30] in the presence of zinc acetate in ethanol or pentanol. ZnPc and H_2Pc were prepared and purified according to the procedure given in ref 31. *tert*-Butyl substitution eases the synthesis of materials and improves their solubility; its effect on the optical absorption spectra is, however, insignificant. On the other hand, the increase in the number of benzo units causes a pronounced shift of the Q-band toward longer wavelengths, which is ascribed to the stronger delocalization of the molecular π-electron system.[32] The center of the

* Corresponding author.
† Present address: Martin-Luther-Universität Halle-Wittenberg, D-06099 Halle, Germany.
‡ Also at Physics Department, Freie Universität Berlin.

10.1021/jp046576i CCC: $30.25
Published on Web 04/05/2005

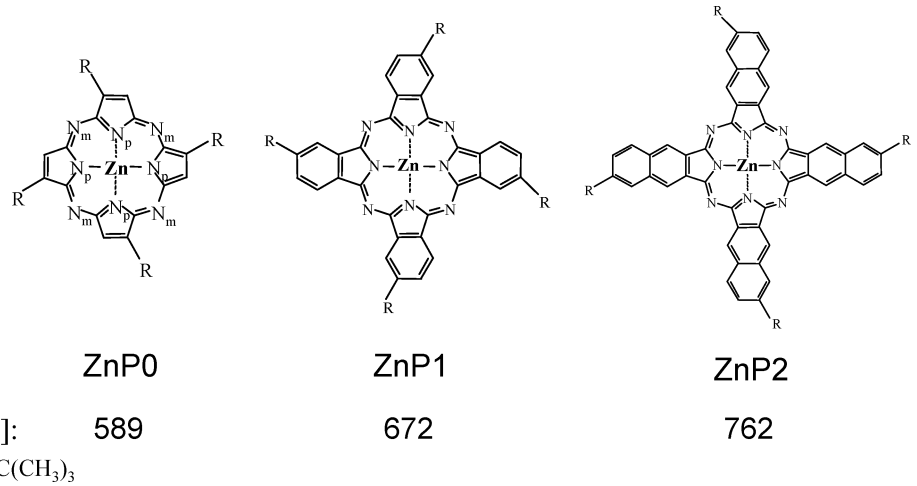

Figure 1. Illustration of the zinc porphyrazine molecules investigated in the present work. R denotes a substituent *tert*-butyl group. The different characters of the nitrogen atoms in the molecules are marked for the ZnP0 molecule: N_p denotes a pyrrole nitrogen atom and N_m denotes a meso-nitrogen atom. The center of the Q-band for each compound dissolved in dioxane is given by λ_{max} (±2 nm uncertainty).

Q-band for each compound dissolved in dioxane is indicated in Figure 1. For ZnTAP (ZnPz),[25,27] ZnPc,[11,12,25,26] and ZnNc[11] the Q-band is primarily attributed to the transition from the a_{1u} HOMO orbital to the e_g LUMO. The assignment of these absorption bands is similar for the *tert*-butyl-substituted molecules.[33]

2.2. Thin Film Preparation and Photoemission Measurements. Thin films of ZnP0, ZnP1, ZnP2, and ZnPc, as well as those of H_2P0, H_2P1, and H_2P2, were deposited by sublimation on an Au(111) single crystal in ultrahigh vacuum (2×10^{-10} mbar base pressure). The materials were evaporated from open quartz crucibles mounted at ca. 5 cm distance from the 10 mm diameter gold substrate. During deposition the crystal was kept at room temperature. Prior to deposition the gold substrate was cleaned by repeated cycles of Ar^+ sputtering and annealing to 750 °C. The gold Au(111) single crystal was mounted on a manipulator which allowed for sample rotation (azimuth, tilt, polar) and translation in front of the energy analyzer used for photoelectron detection. The sublimation temperatures for film preparation, as measured by thermocouples connected to the quartz crucibles, were 195, 400, 500, and 390 °C for ZnP0, ZnP1, ZnP2, and ZnPc, respectively. For H_2P0, H_2P1, and H_2P2 the sublimation temperatures were 180, 350, and 500 °C, respectively. The existence of only intact molecules in the films was confirmed by optical absorption measurements (spectra recorded between 220 and 1100 nm). The absorption spectrum of a given native material dissolved in dioxane and that obtained by dissolving the corresponding film, grown under the actual preparation conditions on a quartz substrate, exhibited no differences. We have also measured the absorption spectra of the remaining material (left in the quartz oven after film preparation) dissolved in dioxane, again observing no effect of decomposition.

The ZnPc films were typically prepared to be about 400 ± 40 Å thick, as determined from the deposition rate monitored by a quartz crystal microbalance. The ZnP0, ZnP1, and ZnP2 films were made to contain about an identical number of molecules by scaling the monitored thickness to the respective molecular mass. Following the film preparation the sample was transferred under ultrahigh vacuum conditions into the analysis chamber for measurements.

The photoemission experiments were performed at the MBI−BESSY beamline (undulator U125) at the synchrotron radiation facility BESSY in Berlin. This beamline has been described in more detail elsewhere.[34] It provided photon energies between 20 and 180 eV. For 64 eV photons the energy resolution was about $E/dE = 6000$, with a photon flux of ca. 4×10^{12} s^{-1} at 100 mA ring current. The analysis chamber (base pressure better than 2×10^{-10} mbar) is equipped with a hemispherical electron energy analyzer, Omicron EA 125. For the present experiments, photoelectrons were detected in normal emission geometry with grazing light incidence (83° with respect to the surface normal) and polarization of the synchrotron light at 80° with respect to the surface normal.

The binding energies reported in the paper were determined with respect to the vacuum level for thin films that also showed the substrate Au 4f levels. For this kind of films the charging was considered negligible. From spectra measured with a negative bias applied to the sample, the low energy cutoff was determined. Based on this, the binding energies were determined via $BE = h\nu - (E_{kin} - E_{cutoff})$, where $h\nu$, E_{kin}, and E_{cutoff} represent the excitation energy, the kinetic energy, and the low energy cutoff of the spectrum. For the thicker films, to compensate for charging, the binding energy scales were aligned to those obtained for the corresponding thin films.

3. Results and Discussion

3.1. Effect of *tert*-Butyl Substituent on Photoemission Spectra. Figure 2 compares the photoemission spectra of ZnP1 and unsubstituted ZnPc, both obtained for 98.7 eV excitation energy. The spectra are normalized to the background. For clarity they are vertically displaced with respect to each other, and in addition, to facilitate the comparison, on top of the ZnP1 spectrum we also present the spectrum of ZnPc (dotted). At first glance the intensities of bands B, E, F, and F′ seem surprisingly high for ZnPc; they appear larger in the ZnPc spectrum than in the ZnP1 one, even though the latter compound contains additional *tert*-butyl groups. As no change of the background shape occurs for the two spectra, the relative intensity of these peaks is attributed to the normalization procedure. More precisely, this is because the normalization of the spectra was done at the background, but the background intensity increases with the *tert*-butyl addition.

The direct comparison of ZnPc and ZnP1 photoemission curves reveals that the *tert*-butyl addition to the ZnPc macrocycle leads to a signal increase at the position of band G and in the 9.5−13.5 eV binding energy region. However, considering the comparison between H_2Pc and H_2P1 spectra[9] and that between

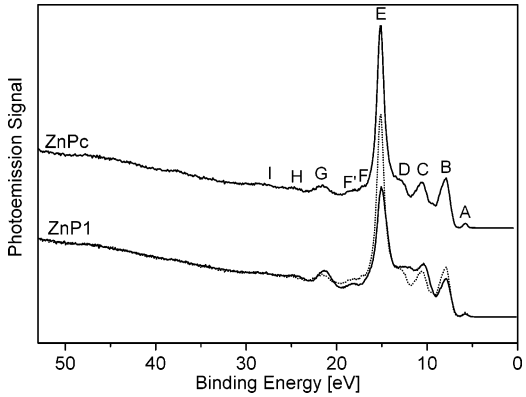

Figure 2. Photoemission spectra of ZnP1 and ZnPc thin films at 98.7 eV photon energy. The dotted line represents the ZnPc spectrum plotted on top of the ZnP1 spectrum. Electron binding energies are given with respect to the vacuum level. Labels and their assignment are discussed in the text.

CuPc and CuP1,[10] it results that *tert*-butyl contributions are also found in the 13.5−16 eV binding energy range. The latter contributions are not observed in the ZnP1−ZnPc spectra comparison due to the significant Zn signal in the respective region and to the normalization procedure.

Generally, the peak positions are roughly the same in ZnPc and ZnP1 spectra. In the ZnP1 spectrum, bands C and G are shifted by about 0.2 eV toward lower binding energies as compared to the ZnPc case. Peaks F and F′, as well as D and C, are no longer well resolved for *tert*-butyl substitution. Good agreement exists between the above-mentioned changes and the modifications appearing in the H_2Pc[9] or CuPc[10] spectra upon *tert*-butyl substitution. Overall, the differences between the photoemission spectra of substituted and unsubstituted compounds are mainly the additional contributions from the *tert*-butyl groups. No significant changes in the electronic valence structure of the macrocycle are detected.

3.2. Peak Assignment and Metal Features in the Spectra. Calculations using D_{4h} symmetry for ZnPc (molecule placed in an *xy*-plane with the axis passing through the pyrrole nitrogen atoms) showed that the HOMO is an a_{1u} orbital having exclusive ligand contributions and π character.[25,26,35,36] It has in fact the same composition (C 2p atomic orbitals) as the HOMO of H_2Pc. In another study, 2% contribution from pyrrole nitrogens, additional to the C 2p character, has been claimed.[12] The HOMO − 1 is calculated to be a b_{1g} orbital with relatively low Zn $d_{x^2-y^2}$ contribution (determined as 12% in ref 12 and 20% in ref 26), but with significant pyrrole nitrogen lone pair (∼66%) and carbon character.[12] A large energy separation (∼1.1 eV[12]) is found between the HOMO − 1 and the HOMO. As determined in ref 12, the HOMO − 2 mainly arises from the meso-bridging nitrogen atoms with some contributions from pyrrole nitrogen and carbon. The very next occupied orbitals are calculated to have mainly mixed contributions from carbon and nitrogen atomic orbitals. The Zn 3d shell is considered to be unperturbed for the low energies of the electronic spectrum. Except for the HOMO − 1, occupied molecular orbitals that include Zn 3d contributions have energies that are separated by 7.96−8.94 eV from the HOMO energy.[12]

In the case of ZnTAP[25] and ZnNc,[29] the HOMO is calculated to derive also from the carbon atomic orbitals. It is an a_{1u} orbital, well separated from the HOMO − 1.

The photoemission curves of ZnP1 and H_2P1 thin films, measured at 89.6 eV excitation energy, are displayed in Figure 3. The spectra have been normalized to achieve the best overlap

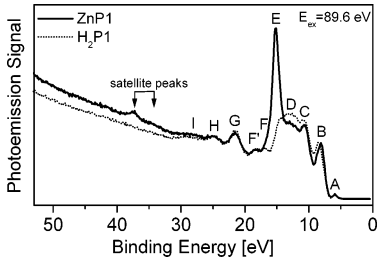

Figure 3. Comparison of photoemission spectra of ZnP1 and H_2P1 thin films.

in the region of band G. In the H_2P1 spectrum the features C and D appear with higher intensities than in the ZnP1 spectrum as a consequence of the normalization procedure. This is because the normalization is done in a region where the photoemission signal is strongly overlapped with the background signal, the latter being larger in the spectra of ZnP1.

In view of the previously mentioned theoretical results, and accounting for the fact that ZnP0, ZnP1, and ZnP2 are chemically very similar to ZnTAP, ZnPc, and ZnNc, respectively, it is concluded that band A in the ZnP1 spectrum in Figure 3 originates from the HOMO of the molecule. To make the assignment of features B, C, and E, we use the calculations for the energies of ZnPc molecular orbitals presented in ref 12. We compared the difference in energy between the various molecular orbitals and the HOMO with the difference in energy between the photoemission peaks and the center of the peak derived from the HOMO (Figure 3). Thus, we deduce that band B includes contributions from several in-plane and π molecular orbitals. As comes out by comparing our results to those from ref 12, the in-plane molecular orbitals that give a photoemission signal at the position of band B are $11b_{1g}$, which is the HOMO − 1; $9b_{2g}$, which is the HOMO − 2; $19e_u$; and $13a_{1g}$. While the HOMO − 1 has strong contributions from the pyrrole nitrogen lone pairs mixed with 12% contributions from the Zn $d_{x^2-y^2}$, each of the other three molecular orbitals is largely derived from the meso-nitrogen lone pairs.[12] The π molecular orbitals that have a photoemission signal at the position of band B are $3b_{2u}$, $6e_g$, $5a_{2u}$, $5e_g$, $2b_{1u}$, $4a_{2u}$, and $1a_{1u}$. Among them, the $4a_{2u}$ molecular orbital has strong contributions from the pyrrole nitrogen and meso-nitrogen atoms; the other π orbitals are derived mainly from benzene and pyrrole carbon. Thus, band B contains a photoemission signal originating from nitrogen, benzene, pyrrole carbon, and Zn, though the latter is in a small amount. We attribute the much higher intensity of band B relative to band A to the fact that band B contains signals from several π and localized molecular orbitals, while band A includes only the emission originating from the HOMO of the molecule. Compared to the H_2P1 case, in the ZnP1 spectrum band B is found at lower binding energy (by ∼0.3 eV). It is likely that this shift results from the fact that in ZnP1 the orbital $11b_{1g}$ is pushed up by antibonding with the Zn $d_{x^2-y^2}$ (see ref 12). Concerning the signal from the $4e_g$ orbital mentioned in ref 12, we interpret that this is found in the border region between peaks B and C. However, band C includes the signal from the $18e_u$ and $17e_u$ in-plane orbitals, which each have 26% pyrrole nitrogen lone pair contributions.[12] The emission from the $10b_{1g}$ orbital, which is derived from benzene, is also found at the position of band C.

Reference 12 does not present the states found between the above-mentioned $17e_u$ orbital and the orbitals that have significant Zn 3d contributions. However, based on the comparison between ZnP1 and ZnPc spectra, it is concluded that also *tert*-butyl signal contributes to band C. Feature D in the spectrum

of ZnP1 appears to have a one-to-one correspondence to that of the analogous metal-free complex, H_2P1.[9] Thus, it contains emission from benzene and *tert*-butyl. As concluded from the comparison of ZnP1 and H_2P1 photoemission spectra and as also results from ref 12, zinc signal is found at the position of band E. This signal was assigned to the direct emission from the Zn 3d level.[37] More exactly, molecular orbitals contributing to band E are $7b_{1g}$, $5b_{2g}$, $8a_{1g}$, $1e_g$, $6b_{1g}$, and $7a_{1g}$. These orbitals include mainly Zn 3d contributions but also some contributions from benzene and from the carbon and nitrogen atoms found in the central ring.[12] As deduced in section 3.1, this band includes also *tert*-butyl signal. Since we find one single band for the Zn 3d photoemission signal, our results support the calculations from ref 12 according to which the Zn 3d level remains almost unperturbed in the low energy part of the electronic spectrum; the only 3d orbital that interacts to a certain extent with the macrocycle is the Zn $d_{x^2-y^2}$. The intensity of band E relative to that of the other bands in the photoemission spectrum rises with increasing photon energy. This is a result of the changes in the cross sections for Zn 3d, C 2s, C 2p, N 2s, and N 2p, with varying photon energy. The cross sections for all these orbitals decrease with increasing excitation energy, but for Zn 3d the decrease is slower.[38] Thus, the ratio between the cross sections for Zn 3d and C 2s, C 2p, respectively N 2s, N 2p, becomes larger with increasing photon energy. Reference 12 does not present calculations for the molecular orbitals that correspond to larger binding energies. The spectra comparison in Figure 3 indicates that the Zn signal extends up to the position of feature F. However, this feature includes also benzene contributions, as in H_2P1 (see ref 9). Because the comparison of ZnP1 and H_2P1 photoemission curves does not indicate the presence of Zn signal at the position of bands F′, G, H, and I, these features appearing to have a one-to-one correspondence in the two spectra, for further peak assignment we use the calculations done for H_2Pc by Orti and Brédas[39] and the results from our previous study on the analogous metal-free compounds.[9] We thus conclude that feature F′ includes signal originating from the 2s orbitals of the C atoms found in the central molecular ring, while peak G contains contributions similar to those from the C 2s $1e_{1u}$ molecular orbital of benzene[39] and *tert*-butyl.[9] Band H contains emission from the same constituents as in the C 2s $1a_{1g}$ molecular orbital of benzene,[39] while band I includes signal from pyrrole nitrogen.[9,39]

The two features marked by arrows and found at binding energies larger than 33 eV in the ZnP1 spectrum shown in Figure 3 are absent in the spectrum of the metal-free compound, and are barely distinguishable in the spectra of ZnPc and ZnP1 at 98.7 eV (Figure 2). These features are assigned to the Zn satellite signal,[37] and are strongly enhanced for the 3p−4s excitation of the central Zn^{2+}.

The spectra of ZnP0, ZnP1, and ZnP2 obtained for 91.7 eV photon energy are plotted in Figure 4. All spectra were normalized to unity at the maximum of peak E and were then vertically translated for clarity.

In the case of ZnP2 we deduce from ref 29 that band A is also derived from the HOMO of the molecule. To the best of our knowledge, calculations similar to those done for ZnPc in ref 12 showing the contributions of individual atoms to the molecular orbitals do not presently exist for ZnNc. However, comparing the photoemission spectra of ZnP1 and ZnP2, we conclude that the ZnP2 peaks include contributions similar to those found for ZnP1 with the difference that the benzene signal is now replaced by the naphthalene one. This affirmation is based also on the study done for metal-free phthalocyanine and naphthalocyanine in ref 40. There it is stated that the electronic structure of the macrocycle is dominated by the electronic levels of the polyacetic units.

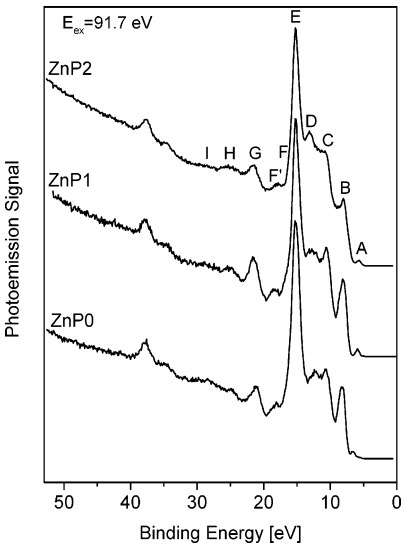

Figure 4. Photoemission spectra (vertically displaced with respect to each other) of zinc porphyrazines in the series. The ligand size increases from bottom to top. Spectra were obtained for 91.7 eV photon energy.

On the basis of the results from ref 25, we deduce that in the ZnP0 spectrum band A also originates from the HOMO of the molecule. In the same study, calculations for several other molecular orbitals of the unsubstituted compound ZnTAP are performed. Comparing the energy of these orbitals relative to the HOMO with the difference in energy between the ZnP0 photoemission peaks and the peak originating from the HOMO, we conclude that the calculated orbitals $7b_{1g}$, $3a_{2u}$, $2b_{2u}$, $7b_{2g}$, $4e_g$, $2a_{2u}$, and $11e_u$ would give signals at the position of band B, the orbital $8a_{1g}$ would give a signal in the border region between peaks B and C, and the emission from the $3e_g$ orbital would contribute to feature C. Clearly, in making the assignment of the ZnP0 photoemission features, the benzene contributions in the spectra must be disregarded and only the contributions from the central C−N ring, pyrrole units, zinc, and *tert*-butyl should be considered.

However, we noted that apparently some disagreements still exist in the literature concerning the calculations of the molecular orbitals and of the atomic contributions to the molecular orbitals for ZnTAP and ZnPc compounds.

3.3. Evolution of the Photoemission Features as a Function of Ligand Size. In Figure 4 one notices that the peaks containing signals from the aromatic units and also the background increase relative to the Zn 3d band with enlarging ligand size.

The position of the Zn 3d main line is identical for all the Zn compounds studied here, 15.2 ± 0.07 eV binding energy. Also the Zn satellite peaks exhibit the same binding energy in ZnP0, ZnP1, and ZnP2 spectra. The changes in the positions of bands H and G with increasing ligand size are consistent with those observed for copper[10] and metal-free[9] compounds. They have constant binding energy for the benzene-containing complexes (ZnP1 and ZnP2). For ZnP0, relative to the ZnP1 case, bands H and G shift toward lower binding energies by ∼0.2 and 0.4 eV, respectively. We interpret that the origin of this shift is the absence of benzene signal in the case of the ZnP0 molecule.

A blowup of the edge of the valence region is presented in Figure 5. As for the case of the metal-free[9] and copper[10] compounds, a binding energy decrease of feature A (derived

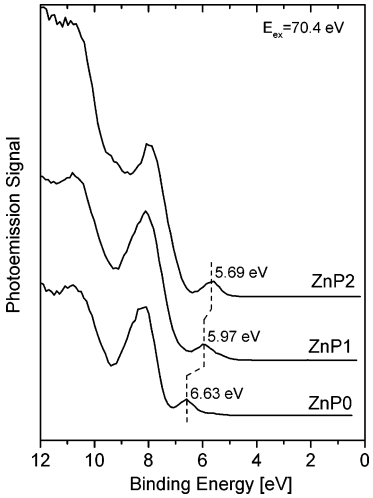

Figure 5. Photoemission spectra of ZnP0, ZnP1, and ZnP2 thin films in the HOMO region. Labels mark the respective HOMO binding energies.

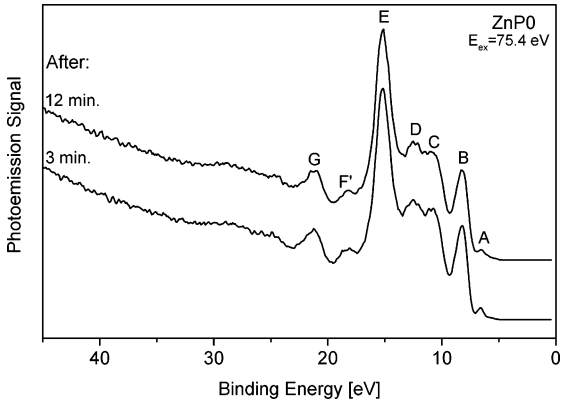

Figure 6. Photoemission spectra of a ZnP0 thin film, measured on an identical surface spot after different exposure times to synchrotron radiation.

from the HOMO) is observed for increasing ligand size. The HOMO binding energies are determined to be 6.63 ± 0.07, 5.97 ± 0.07, and 5.69 ± 0.07 eV for ZnP0, ZnP1, and ZnP2, respectively. Because for these zinc compounds the HOMO has an atomic orbital composition similar to that of the HOMO for the corresponding metal-free compounds (see refs 25, 26, and 40 on unsubstituted ZnPc and H_2Pc), its destabilization upon linear benzoannelation must have the same origin in the two classes of molecules. As shown in ref 40, the HOMO is mainly localized on the central porphyrazine ring, and the antibonding interactions with the fused benzo units at linear benzoannelation cause a decrease of its binding energy. As these interactions are weaker for the outer benzene units than for the inner ones, the difference in HOMO binding energy between ZnP2 and ZnP1 is smaller than the one between ZnP1 and ZnP0. The difference in HOMO binding energy between any two compounds in the Zn series is nearly the same as for the corresponding metal-free complexes.

Additionally, band B shifts slightly with the extension of the ligand, yielding binding energies of 8.2 ± 0.07, 8.1 ± 0.07, and 8.00 ± 0.07 eV for ZnP0, ZnP1, and ZnP2, respectively. This is likely to reflect the effect of benzene contributions, which gradually increase with ligand size.

To further characterize the Zn series of molecules, in addition to the investigations with extreme ultraviolet (EUV) light, X-ray photoelectron spectroscopy (XPS) using nonmonochromatized Al Kα radiation (main excitation energy $h\nu = 1486.7$ eV) was performed. The main focus in the XPS studies was on the analysis of the N 1s and Zn 2p core level regions, since these are particularly sensitive to changes in the Zn−N bonding character. However, within the experimental error bars (~0.2 eV) the XPS measurements showed no changes in the separation between C 1s and N 1s or C 1s and Zn $2p_{1/2,3/2}$ peaks with increasing ligand size.

3.4. Photostability. To examine the photostability of these zinc compounds, photoemission spectra were recorded for different synchrotron radiation exposure times. Spectral changes induced by the synchrotron radiation need to be identified to allow for a meaningful analysis and interpretation of the measured data.

Figure 6 presents the photoemission spectra of a ZnP0 thin film obtained from an identical surface spot but for different synchrotron radiation exposure times. Peak A is one of the strongly changing features in the ZnP0 photoemission spectrum as a result of photodegradation. It smears out and broadens, and eventually for long exposures it appears only as a shoulder in the spectra. Features B, C, D, F′, and G broaden and smear out with a lower rate than peak A. The Zn satellite peaks are not significantly affected by irradiation, as inferred from the spectra of ZnP0 at 91.7 eV photon energy. The changes of the ZnP1 spectrum occur for longer irradiation times as compared to ZnP0 (data not presented here), and manifest themselves by weaker similar modifications. ZnP2 is the most stable compound within the series with respect to synchrotron radiation exposure.

Very similar photostability trends were observed for the respective metal-free[9] and copper[10] compounds. Since ZnP0 is the most sensitive compound with respect to synchrotron radiation exposure, the central porphyrazine ring appears to be most strongly affected by photodegradation. A possible explanation for these changes is the breaking of bonds in the molecule as a result of irradiation with EUV photons. Irrespective of the different photosensitivities, measurements were, however, always performed by frequently changing the exposed sample spot.

3.5. Zinc Satellites. As the photon energy is increased from 86 to 101 eV, one notices in the photoemission spectra a growth and subsequent decrease of the zinc satellite peaks that are found at approximately 34.8 and 37.8 eV binding energy. For the excitation energies used in the present experiments, the maximum intensity of these peaks occurs for 91.7 eV. The photoemission spectra of ZnP0, ZnP1, and ZnP2 films obtained for 91.7 and 87.1 eV excitation energy are displayed in Figure 7. The inset presents photoemission spectra (smoothed by adjacent average) of the ZnP0 thin film in the region of the satellite peaks, for several photon energies. These spectra were normalized to the signal for 30 eV binding energy and were then vertically translated for clarity. The inset allows direct tracing of the evolution of the satellite intensity as a function of photon energy. For all of the present zinc compounds, the satellite features are clearly observed only for excitation energies around 91.7 eV.

A blowup of the zinc satellite region for ZnPc and ZnP1 spectra measured at 86.6, 91.7, and 100.2 eV is displayed in Figure 8. For ZnPc also the 85.6 eV spectrum is shown. One can note that the ZnPc spectrum exhibits a weak zinc satellite signal for 85.6, 86.6, and 100.2 eV excitation, while for the same photon energies satellite features are not distinguishable for ZnP1. A behavior similar to that of ZnP1 is also found for ZnP0 and ZnP2. We conclude that in the photoemission spectra of ZnP0, ZnP1, and ZnP2 for 86.6 and 100.2 eV excitation, the satellites are masked by the larger background as compared to the ZnPc case. A reduced background signal (as for ZnPc)

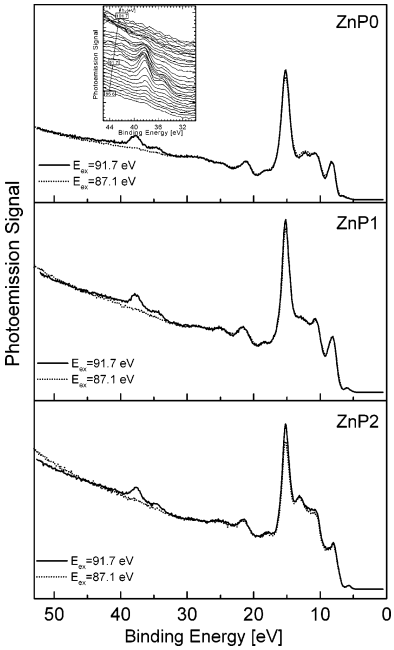

Figure 7. Photoemission spectra of ZnP0, ZnP1, and ZnP2 thin films for 91.7 eV (solid lines) and 87.1 eV (dotted lines) photon energy. The inset shows photoemission spectra (smoothed by adjacent average) of the ZnP0 thin film in the region of the satellite peaks, obtained for several photon energies (from bottom to top: 86.6, 87.1, 87.6, 88.1, 88.6, 89.1, 89.6, 90.1, 90.6, 91.1, 91.7, 92.2, 92.7, 93.2, 93.7, 94.2, 94.7, 95.1, 95.7, 96.2, 96.8, 97.2, 97.8, 98.2, 98.7, 99.2, 99.8, 100.2, 101.2, 101.7 eV). Those spectra are normalized to the signal for 30 eV binding energy and vertically translated.

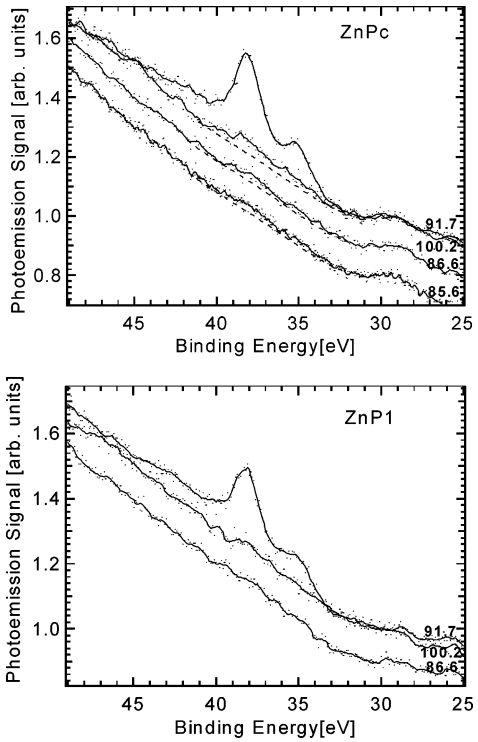

Figure 8. Photoemission spectra of ZnPc and ZnP1 thin films in the region of zinc satellite peaks, obtained for 86.6, 91.7, and 100.2 eV photon energy. For ZnPc also the spectrum measured at 85.6 eV is shown. The dashed lines in the upper panel serve to guide the eye.

makes the satellites better observable over a larger range of excitation energies.

It is generally accepted that in ZnPc the zinc atom is divalent,[12,26] which implies a Zn $3p^6 3d^{10} 4s^0$ formal configuration in the molecular ground state. Nevertheless, due to the fact that the bonding between metal and ligand is not purely ionic, having also a covalent character, the 4s and 4p orbitals get partially occupied. Thus, in ref 26 the charge distribution is calculated to be $3d^{10}4s^{0.55}4p^{0.81}$. However, the next discussion in this paper will consider just the formal configuration for the central Zn atom.

ZnP0, ZnP1, and ZnP2 are similar in chemical structure and properties to ZnPc, which implies that the central zinc is also divalent in these porphyrazine compounds. The above-mentioned zinc satellite peaks were previously observed for ZnPc[37] and ZnO.[41] They arise from a 3d ionization process with shakeup, which leads to a formal $3d^8 4s^1$ final-state configuration of zinc (two holes in the Zn 3d shell and one electron in the 4s level):[42]

$$3p^6 3d^{10} 4s^0 + h\nu \rightarrow 3p^6 (3d^8 4s^1) + e^-$$

The enhancement of the satellite peaks observed for photon energies around 91.7 eV is a result of the Zn 3p−4s excitation accompanied by an Auger decay of a 3d electron, with the emission of another electron from the 3d level.

Actually, for the particular case of ZnPc a similar interpretation was previously proposed, but treating the central zinc as quasiatomic.[37] As claimed by the authors, the s−p hybridization would lead to empty 4s states which, in the presence of a core hole, are localized. Then the existence of two satellite peaks was attributed to the $3d^8$ multiplets.[37] In contrast, we stress that the enhancement of the Zn satellite peaks in ZnPc (and ZnP0, ZnP1, ZnP2) spectra indeed arises from the 3p−4s excitation accompanied by an Auger decay of a 3d electron, but the holes in the Zn 4s level exist mainly because the central zinc has a formal Zn^{2+} oxidation state.

In a simple model[37] this process can be schematically described as

$$3p^6 3d^{10} 4s^0 + h\nu \rightarrow 3p^5 3d^{10} 4s^1 \leftrightarrow 3p^6 3d^8 4s^1 + \text{Auger electron}$$

so the obtained final state is again $3d^8 4s^1$. Thus, an identical final state of the system is reached by ionization with shakeup and through the Zn 3p−4s excitation. Consequently, the coherent superposition of the electron emerging from photoionization with shakeup and of the Auger electron occurs, and leads to the enhancement of the satellite peaks.

In addition to the satellite features, above the threshold energy, $M_{2,3}M_{4,5}M_{4,5}$ Auger peaks appear.[37] In the present series of spectra they are observed on the high binding energy side of the satellites for excitation energies equal to or exceeding 91.7 eV (see Figures 7 and 8). The Auger signal is not clearly distinguished in the spectra, and therefore these features will not be further examined here. We notice, though, that the Auger signal in the vicinity of the satellite peaks complicates the analysis of the data.

To get information about the satellite intensity dependence on the excitation energy, we have fitted the respective region of the photoemission spectra. The fit function was a sum of two Gaussians of equal widths, 1.07 eV, and a constant separation of 3 eV between their centers (accounting for the satellite peaks) plus a linear function (accounting for the background signal in that region). Both the widths of the satellite peaks and their energy spacing were thus fixed parameters for the fit. Their values have been determined from the analysis of the data measured at excitation energies where the satellite peaks are well observed but no Auger signal is detected. Figure 9

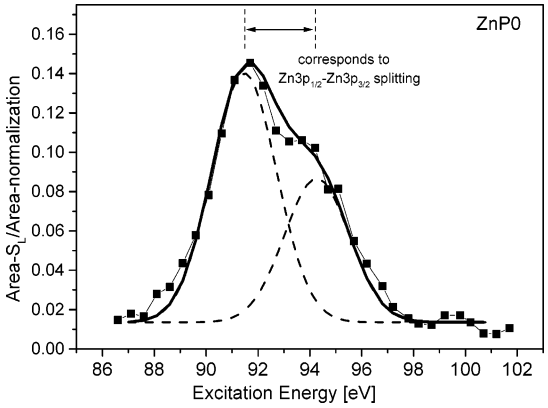

Figure 9. Area of the largest zinc satellite peak normalized to the background intensity as a function of excitation energy for ZnP0.

shows for ZnP0 the area of the largest zinc satellite peak (Area-S_L) normalized to the background intensity as a function of excitation energy. Similar dependencies were also obtained for ZnP1 and ZnP2, and also for the sum of both satellite peak areas. The curve in Figure 9 exhibits a double peak structure and can be well fitted by a superposition of two Gaussians of equal widths, separated by 2.8 eV. This indicates the excitation of the spin−orbit split components $3p_{1/2}$ and $3p_{3/2}$ of the Zn 3p level. Due to the inaccuracies in the fitting procedure, Figure 9 shows overestimated values of the satellite areas for off-resonant excitations, when practically no satellite peak is observed by direct examination of the ZnP0, ZnP1, or ZnP2 spectra.

The resonance curves for ZnP0 (Figure 9), ZnP1, and ZnP2 were obtained by normalization of the satellite areas with respect to the background signal, which has different intensities for the three compounds. Hence, these curves are not suited for analyzing the variations in the satellite intensity as a function of ligand size. This information can, however, be accessed by comparing the ratios between the area of the satellite signal and the area of the Zn 3d direct photoemission signal, for the different molecules in the series.

To determine the area of the Zn 3d contributions, the ligand signal was extracted from the measured Zn porphyrazine spectra. First, a background that had a Shirley and a linear component was subtracted from both the Zn compound and the corresponding metal-free compound spectra. This combination of a linear plus Shirley-type background was found to account best for the experimental data. In a next step, for a given excitation energy, each metal-free compound spectrum (after background subtraction) was overlapped at the ligand features with the corresponding zinc compound spectrum (also background subtracted). Subsequently, the metal-free compound spectrum was subtracted from the one of the zinc compound, and the difference spectrum was integrated at the position of the Zn 3d main line. Identical integration ranges were assured for all compounds at all excitation energies. The procedure is illustrated in Figure 10, which shows the overlapped ZnP2 and H_2P2 spectra (both after background subtraction) and the difference spectrum obtained for 94.2 eV photons.

The ratios between the area of the larger Zn satellite peak (Area-S_L) and the area of the Zn 3d main line (Area-Zn3d) as a function of excitation energy for ZnP0, ZnP1, and ZnP2 are displayed in Figure 11. The same type of dependencies were also obtained for the ratios between the summed areas of both satellite peaks and the area of the Zn 3d main line. Error bars are only shown for ZnP2 in several points, but they are calculated to be similar for all three compounds. One can see in Figure 11 that for a given excitation energy below 91.7 eV

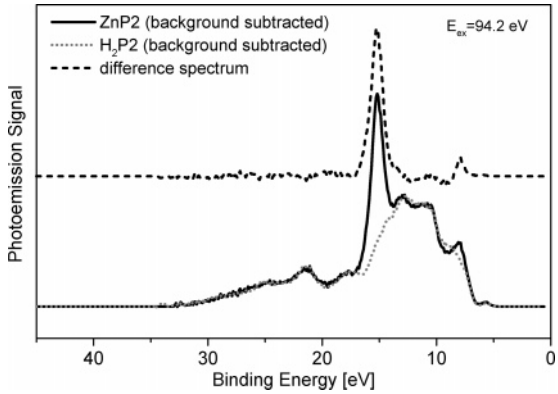

Figure 10. Overlapped ZnP2 and H_2P2 spectra, both after background subtraction (bottom), and their difference curve, obtained by subtracting the H_2P2 spectrum from the ZnP2 one (top).

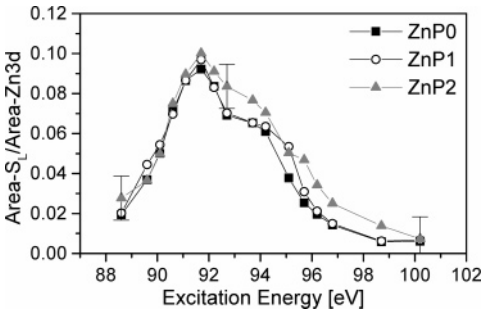

Figure 11. Ratios between the area of the largest zinc satellite peak and the area of Zn 3d main line for ZnP0, ZnP1, and ZnP2.

the intensity ratios are nearly identical for ZnP0, ZnP1, and ZnP2, while for higher photon energies larger values are obtained for ZnP2 than for the other two compounds. We attribute the enhancement of the ZnP2 ratios to an artifact generated by the following reason. For photon energies equal to or exceeding 91.7 eV Auger peaks appear in the spectra. The Auger signal in the close vicinity to the satellite peaks introduces additional inaccuracies in the spectral analysis (not included in the error bars from Figure 11). Consequently, the different values of the satellite-to-main line intensity ratios for ZnP2 are likely to result from a less precise estimation of the satellite areas within the fitting procedure. We thus conclude that, within our accuracy, the satellite-to-main line intensity ratios in the present measurements are identical for ZnP0, ZnP1, and ZnP2. This would suggest the existence of an equal number of free 4s states for all three compounds.

As previously mentioned, in ZnPc, although the metal atom has a formal charge of +2, the 4s and 4p orbitals are partially populated (the charge distribution calculated in ref 26 is $3d^{10}4s^{0.55}4p^{0.81}$). Similar to the case of other metal phthalocyanines, the fact that there is charge on 4s and 4p indicates that the bonding between metal (Zn) and Pc ligand is not purely ionic but significantly covalent.[26] Therefore, our photoemission studies provide no indication of any difference in the degree of covalent (or ionic) character of the Zn−ligand bond when comparing ZnP0, ZnP1, and ZnP2.

This behavior is different from that observed for the analogous set of copper porphyrazines. In the latter system, an increase in the ionic character of the Cu−N bond with increasing ligand size was inferred experimentally.[10] Therefore, we expected a similar effect also for the zinc series of porphyrazines, which should have resulted in an increased ratio between the zinc shakeup satellites and zinc main line with the enlargement of the ligand (because more free Zn 4s states exist if the Zn−N

bond becomes more ionic). Note, however, that in analyzing the intensity variations of the zinc satellite peaks we are less sensitive than in the case of the copper satellites. For the copper porphyrazines, the satellites from the valence band were sufficiently intense to reveal a dependence with the ligand size even at off-resonant excitations. Off-resonance, the Zn shakeup satellites have too small an intensity to be well observed in the spectra, and therefore their analysis can be done only on-resonance. However, within our accuracy the resonant increase of the Zn shakeup satellites does not differ for ZnP0, ZnP1, and ZnP2. Whether a change in the Zn−N bond character is simply too small to be detected in the present photoemission measurements or whether it is really absent remains unresolved at the present moment.

4. Conclusions

The analysis of the photoemission spectra of thin films of benzoannelated zinc porphyrazine molecules deposited on a gold single crystal has been performed. The focus was on the evolution of the electronic structure and of the zinc−ligand interactions with increasing ligand size. The measurements revealed that the enlargement of the ligand system causes a shift of the HOMO toward lower binding energies, which is similar to that observed for the analogous metal-free compounds. Zinc shakeup satellite signal is clearly observed in the spectra of the valence region for photon energies near the 3p−4s resonant excitation. However, for off-resonant excitations the satellite peaks were observable only in the ZnPc spectrum, with an intensity of at most 2% compared to that of the main line. For a given excitation energy, the intensity ratios between the satellite peaks and the Zn 3d main line are similar for ZnP0, ZnP1, and ZnP2. Thus, differences in the covalent (or ionic) character of the bond between zinc and ligand as a function of ligand size were not detected in the present measurements.

References and Notes

(1) *Phthalocyanines. Properties and Applications*; Leznoff, C. C., Lever, A. B. P., Eds.; VCH: New York, 1989; Vol. 1.
(2) *Phthalocyanines. Properties and Applications*; Leznoff, C. C., Lever, A. B. P., Eds.; VCH: New York, 1993; Vol. 3.
(3) Reimers, J. R.; Lu, T. X.; Crossley, M. J.; Hush, N. S. *Chem. Phys. Lett.* **1996**, *256*, 353.
(4) Tomiyama, T.; Watanabe, I.; Kuwano, A.; Habiro, M.; Takane, N.; Yamada, M. *Appl. Opt.* **1995**, *34*, 8201.
(5) Ali, H.; van Lier, J. E. *Chem. Rev.* **1999**, *99*, 2379.
(6) Hanack, M.; Durr, K.; Lange, A.; Barcina, J. O.; Pohmer, J.; Witke, E. *Synth. Met.* **1995**, *71*, 2275.
(7) Nalwa, H. S.; Hanack, M.; Pawlowski, G.; Engel, M. K. *Chem. Phys.* **1999**, *245*, 17.
(8) Nalwa, H. S.; Kakuta, A.; Mukoh, A. *J. Phys. Chem.* **1993**, *97*, 1097.
(9) Pop, D.; Winter, B.; Freyer, W.; Hertel, I. V.; Widdra, W. *J. Phys. Chem. B* **2003**, *107*, 11643.
(10) Pop, D.; Winter, B.; Freyer, W.; Weber, R.; Widdra, W.; Hertel, I. V. *J. Phys. Chem. B* **2004**, *108*, 9158.
(11) Kobayashi, N.; Mack, J.; Ishii, K.; Stillman, M. J. *Inorg. Chem.* **2002**, *41*, 5350.
(12) Ricciardi, G.; Rosa, A.; Baerends, E. J. *J. Phys. Chem. A* **2001**, *105*, 5242.
(13) Schechtman, B. H.; Spicer, W. E. *J. Mol. Spectrosc.* **1970**, *33*, 28.
(14) Edwards, L.; Gouterman, M. *J. Mol. Spectrosc.* **1970**, *33*, 292.
(15) Huang, T. H.; Rieckhoff, K. E.; Voigt, E. M. *J. Phys. Chem.* **1981**, *85*, 3322.
(16) Stillman, M. J.; Nyokong, H. Absorption and Magnetic Circular Dichroism spectral Properties of Phthalocyanines. In *Phthalocyanines. Properties and Applications*; Leznoff, C. C., Lever, A. B. P., Eds.; VCH: New York, 1989; Vol. 1, p 133.
(17) Nyokong, T.; Gasyna, Z.; Stillman, M. J. *Inorg. Chem.* **1987**, *26*, 1087.
(18) Vancott, T. C.; Rose, J. L.; Misener, G. C.; Williamson, B. E.; Schrimpf, A. E.; Boyle, M. E.; Schatz, P. N. *J. Phys. Chem.* **1989**, *93*, 2999.
(19) Mack, J.; Stillman, M. J. *J. Phys. Chem.* **1995**, *99*, 7935.
(20) Plows, F. L.; Jones, A. C. *J. Mol. Spectrosc.* **1999**, *194*, 163.
(21) Weiss, C.; Kobayashi, H.; Gouterman, M. *J. Mol. Spectrosc.* **1965**, *16*, 415.
(22) Schaffer, A. M.; Gouterman, M.; Davidson, E. R. *Theor. Chim. Acta* **1973**, *30*, 9.
(23) Soares, L. D.; Trsic, M.; Berno, B.; Aroca, R. *Spectrochim. Acta A* **1996**, *52*, 1245.
(24) Hashimoto, T.; Choe, E. K.; Nakano, H.; Hirao, K. *J. Phys. Chem. A* **1999**, *103*, 1894.
(25) Nguyen, K. A.; Pachter, R. *J. Chem. Phys.* **2001**, *114*, 10757.
(26) Liao, M. S.; Scheiner, S. *J. Chem. Phys.* **2001**, *114*, 9780.
(27) Baerends, E. J.; Ricciardi, G.; Rosa, A.; van Gisbergen, S. J. A. *Coord. Chem. Rev.* **2002**, *230*, 5.
(28) Liao, M. S.; Scheiner, S. *J. Comput. Chem.* **2002**, *23*, 1391.
(29) Kobayashi, N.; Ogata, H. *Eur. J. Inorg. Chem.* **2004**, 906.
(30) Freyer, W.; Mueller, S.; Teuchner, K. *J. Photochem. Photobiol. A: Chem.* **2004**, *163*, 231.
(31) Barrett, P. A.; Dent, C. E.; Linstead, R. P. *J. Chem. Soc. [London]* **1936**, 1719.
(32) Kobayashi, N.; Nakajima, S.; Osa, T. *Inorg. Chim. Acta* **1993**, *210*, 131.
(33) Konami, H.; Hatano, M. *Chem. Lett.* **1988**, 1359.
(34) Gatzke, J.; Winter, B.; Quast, T.; Hertel, I. V. *Proc. SPIE* **1998**, *3464*, 14.
(35) Cheng, W. D.; Wu, D. S.; Zhang, H.; Chen, J. T. *Phys. Rev. B* **2001**, *64*, 125109.
(36) Schlettwein, D.; Hesse, K.; Gruhn, N. E.; Lee, P. A.; Nebesny, K. W.; Armstrong, N. R. *J. Phys. Chem. B* **2001**, *105*, 4791.
(37) Iwan, M.; Koch, E. E.; Chiang, T. C.; Himpsel, F. J. *Phys. Lett. A* **1980**, *76*, 177.
(38) Yeh, J.-J. *Atomic Calculations of Photoionization Cross Sections and Asymmetry Parameters*; Gordon and Breach: Langhorne, PA, 1993.
(39) Orti, E.; Brédas, J.-L. *J. Am. Chem. Soc.* **1992**, *114*, 8669.
(40) Orti, E.; Crespo, R.; Piqueras, M. C.; Tomas, F. *J. Mater. Chem.* **1996**, *6*, 1751.
(41) Didziulis, S. V.; Cohen, S. L.; Butcher, K. D.; Solomon, E. I. *Inorg. Chem.* **1988**, *27*, 2238.
(42) Ishii, T.; Taniguchi, M.; Kakizaki, A.; Naito, K.; Sugawara, H.; Nagakura, I. *Phys. Rev. B* **1986**, *33*, 5664.